Title

An Integrated Damage, Visual, and Radar Analysis of the 2013 Moore, Oklahoma, EF5 Tornado

Journal

Bulletin of the American Meteorological Society, 95(10)

ISSN

0003-0007

Authors

Atkins, Nolan T
Butler, Kelly M
Flynn, Kayla R
et al.

Publication Date

2014-10-01

DOI

10.1175/bams-d-14-00033.1

Peer reviewed

AN INTEGRATED DAMAGE, VISUAL, AND RADAR ANALYSIS OF THE 2013 MOORE, OKLAHOMA, EF5 TORNADO

BY NOLAN T. ATKINS, KELLY M. BUTLER, KAYLA R. FLYNN, AND ROGER M. WAKIMOTO

An analysis of the historic 20 May 2013 EF5 Moore Oklahoma tornado reveals details on the relationship between the damage path and the visual and radar-detected characteristics of the tornado.

The most violent of all tornadoes, those rated F5 (Fujita 1971) or EF5 on the recently created enhanced Fujita (EF) scale (WSEC 2006), are a rare occurrence. Only 0.13% of all tornadoes observed from 1950 to 2007 over the contiguous United States were rated F5 or EF5 (Simmons and Sutter 2011). Yet, their economic and societal impacts are devastating. Adjusted for inflation (constant 2014 dollars), the F5 Bridge Creek–Moore, Oklahoma, tornado on 3 May 1999 produced $1.3 billion in damage (Brooks and Doswell 2001). During the recent 2011 tornado season, the EF5 Joplin tornado resulted in 158 direct fatalities (Simmons and Sutter 2012) and approximately $3 billion in insured losses (Simmons et al. 2013).

The value of performing tornado damage surveys is well established (Fujita 1981; Bluestein and Golden 1993). It is particularly important to survey high-impact events as has been done in the past for the 3 May 1999 Moore–Bridge Creek, Oklahoma (Marshall 2002; Speheger et al. 2002), 4 May 2007 Greensburg, Kansas (Marshall et al. 2008b), 22 May 2011 Joplin, Missouri (NOAA 2011), and 27 April 2011 Tuscaloosca–Birmingham, Alabama (Karstens et al. 2013), tornadoes and many other historical cases. Much has been learned from these and other damage survey studies regarding the low-level tornado wind field (Karstens et al. 2013) and attendant damage (Wurman and Alexander 2005), structure failure (Marshall 2002; Marshall et al. 2008a), distribution of risk in the damage path (Abbey and Fujita 1975; Speheger et al. 2002), nonlinear damage markings (Wakimoto et al. 2003; Marshall et al. 2008b), and the relationship between the condensation funnel, the damage path, and radar observations (Wakimoto et al. 2003).

On 20 May 2013, an EF5 tornado formed over northern Newcastle, Oklahoma, and subsequently moved east-northeast into Moore. The tornado eventually dissipated in the rural countryside just west of Stanley Draper Lake. This is the third violent

AFFILIATIONS: ATKINS, BUTLER, AND FLYNN—Department of Atmospheric Sciences, Lyndon State College, Lyndonville, Vermont; WAKIMOTO—Department of Atmospheric and Oceanic Sciences, University of Colorado Boulder, Boulder, Colorado
CORRESPONDING AUTHOR: Nolan T. Atkins, Lyndon State College, Department of Atmospheric Sciences, 1001 College Rd., Lyndonville, VT 05851
E-mail: nolan.atkins@lyndonstate.edu

The abstract for this article can be found in this issue, following the table of contents.
DOI:10.1175/BAMS-D-14-00033.1

In final form 1 July 2014

(F/EF4 or greater) tornado that has impacted the greater Moore area since 1999. The economic and societal impacts of the 2013 Moore tornado are significant. The tornado is responsible for 24 fatalities (www.ncdc.noaa.gov/stormevents/). Total damage loss is estimated to be $2 to $3.5 billion (www.propertycasualty360.com/2013/05/28/2-35b-in-insured-losses-from-moore-oklahoma-tornad) by Risk Management Solutions. Of the 4,531 damaged structures, 78% are residential buildings assessed at approximately $400 million. Tragically, two elementary schools within the city of Moore, Briarwood Elementary and Plaza Towers, were destroyed by the tornado. Seven of the fatalities were children in the Plaza Towers Elementary School. The Moore Medical Center was also destroyed by the tornado.

Comprehensive and independent ground and aerial damage surveys were conducted in the days and weeks after the event. Synthesis of the damage survey data, visual observations, and dual-polarized Twin Lakes (KTLX) radar data allows for the following two objectives to be investigated. The first is to document the damage produced by this historic event and examine the spatial relationship between the damage, visual characteristics, and dual-polarization observations of the tornado. The second is to quantitatively compare results from independent aerial and ground damage surveys. This objective is especially relevant, as recent studies have begun to examine the utility of satellite and aerial data to supplement and possibly replace ground surveys (Edwards et al. 2013).

DATA ANALYSIS METHODOLOGY.

Damage survey. Independent ground and aerial surveys commenced immediately after the Moore tornado. Detailed aerial surveys were performed on 21[1] and 22 May 2013. The aerial survey on 22 May 2013 was performed by the authors in a Cessna 172 aircraft flown at approximately 305, 1220, and 1830 m above ground level (AGL). A total of 1,177 high-resolution digital single-lens reflex (SLR) photographs were taken as the aircraft slowly circled over the damage path for approximately four hours. Damage in the photographs was then plotted onto 7.5-min-scale U.S. Geological Survey (USGS) topographic maps and in ArcGIS. The National Weather Service EF kit (LaDue and Mahoney 2006) was used to give damage points an EF value. Satellite and street view imagery available in Google Earth were also used extensively to ascertain the type of structures in some of the most heavily damaged areas. Directions of tree fall, debris, and tornado swath marks were also plotted using the aerial photos and 15-cm resolution satellite imagery taken on 21 May 2013, viewable in Google Earth.

An independent ground survey of the 2013 Moore tornado was completed by teams affiliated with the National Weather Center (Burgess et al. 2014). Data from the independent ground and aerial surveys were then checked for consistency. The two surveys were merged to produce a comprehensive and consistent map of the damage path. (All of the aerial damage survey imagery and analyses are available at http://meteorology.lyndonstate.edu/vortex2/Moore2013.)

Photogrammetry. While photogrammetry and research teams equipped with mobile radars were operable on 20 May 2013, they did not deploy on the Moore storm since it would have required deployment in urban areas.[2] Social media were used to collect imagery and video from amateur storm chasers and news crews. Azimuth and elevation grids were superimposed on select photographs and video frames using photogrammetric techniques that are well documented in the literature (e.g., Rasmussen et al. 2003; Zehnder et al. 2007; Wakimoto et al. 2011; Atkins et al. 2012). By measuring the azimuth angles of known landmarks in the photos, the grid uncertainty is estimated to be 0.1°.

It is possible to estimate the condensation funnel diameter (e.g., Wakimoto et al. 2003; Atkins et al. 2012) by triangulation in concurrent photos taken at two or more vantage points. Unfortunately, triangulation is not possible with the available photos of the Moore tornado. The funnel diameter may also be estimated by measuring the azimuth angle ϕ across the funnel and the range R from the photographer to the condensation funnel. To estimate the range from the photographer to the tornado, it is assumed that the condensation funnel center is collocated with the damage path centerline. Uncertainty in the funnel diameter calculation is dependent on R and associated uncertainty δR. It also depends on the uncertainty $\delta\phi$ in the azimuth angle across the funnel, estimated to be 0.2°. The photographer GPS locations were independently verified by a site survey after the Moore event. By using the available GPS coordinates provided by the photographers along with the locations of objects in the background and foreground of the respective photos, the photographer locations were determined to within 1.5 m.

[1] NOAA personnel performed a helicopter aerial survey on 21 May 2013.

[2] The University of Oklahoma Advanced Radar Research Center deployed the mobile PX-1000 X-band radar on the Moore tornado. Data and deployments are summarized in Kurdzo et al. (2014).

Uncertainty in the damage path location is estimated to be 10 m. Therefore, δR is approximately 11.5 m.

Radar data. While there were a number of radars operated by the University of Oklahoma (OU), the National Oceanic and Atmospheric Administration (NOAA), and the Federal Aviation Administration (FAA) that collected data on the Moore tornado, the dual-polarized Weather Surveillance Radar-1988 Doppler (WSR-88D) KTLX data were chosen for analysis. The radar reflectivity and copolar cross-correlation coefficient were objectively analyzed to a Cartesian grid using a two-pass Barnes filter (Koch et al. 1983). The filter and grid parameters were chosen based on the data resolution δ at the range of the tornado. The KTLX data are oversampled every 0.5° in azimuth. The range from the radar to the tornado varied from 30.6 km at 1955:27 UTC (near the time of tornadogenesis; hereafter all times are UTC) to 11.9 km at 2033:46 UTC (near the time of tornado demise). This results in δ varying from 0.534 to 0.208 km. The smoothing parameter [$k = (1.33\delta)^2$; Pauley and Wu 1990] and grid spacing ($\Delta = \delta/2.5$; Koch et al. 1983) were set appropriately. Only the 0.5° elevation angle scan was included in the analysis as we are most interested in the low-level spatial relationship between the TDS, condensation funnel, and the damage track.

RESULTS. *Damage survey, visual, and radar observations.* The Moore tornado begins producing EF0 damage in northern Newcastle at approximately 1956 UTC (Fig. 1).[3] The tornado subsequently moves east-northeast passing through the city of Moore, eventually dissipating 4 km east of the Moore city limits. EF2 damage is observed along nearly the entire damage path. EF3 and EF4 damage is observed within 1.6 km (4 min) of the beginning of the damage path. The damage path abruptly widens after the tornado passed east of U.S. Interstate 44 in south Oklahoma City. EF3 and EF4 damage is observed nearly continuously for approximately 13 km beginning just

[3] Damage (EF0) consistent with weak tornadic rotation was observed up to 5.2 km to the southwest of the damage path start in Fig. 1.

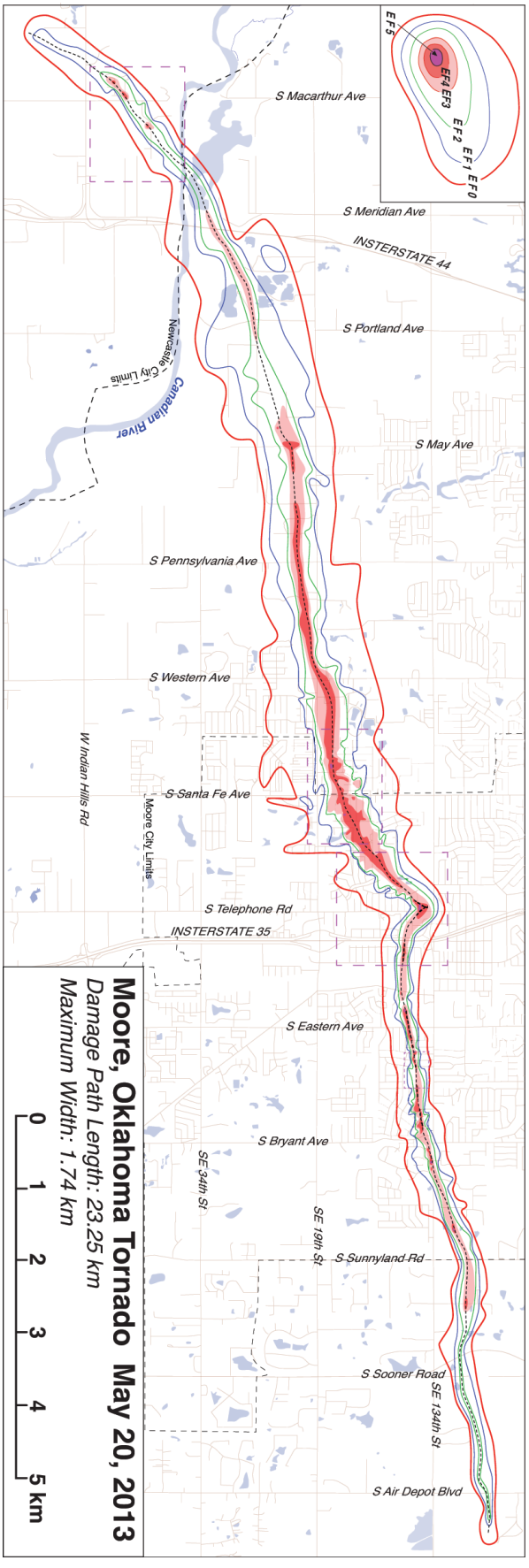

FIG. 1. Damage survey analysis of the 20 May 2013 Moore, Oklahoma, tornado. EF-scale isopleths are shown along with roads (brown) and city boundaries (dashed lines). The black dashed line is the tornado centerline. The dashed magenta boxes are the areas shown in Figs. 2, 4, 5, and 6.

west of South May Avenue. Much of this damage is produced in rural portions of south Oklahoma City and suburban neighborhoods in Moore. EF4 damage is observed at the Briarwood and Plaza Towers Elementary Schools and in suburban neighborhoods in Moore. Two homes just east of the Briarwood Elementary School are rated EF5 by the National Weather Center teams. A prominent cusp in the damage path is located just west of U.S. Interstate 35, also associated with EF5 damage. A small loop of the tornado centerline is observed within the cusp and is inferred by debris furrowing (shown in more detail in Fig. 5). Rapidly updating mobile Doppler radar measurements confirm that the tornado couplet location loops within the cusp just west of U.S. Interstate 35 (Kurdzo et al. 2014). As the tornado moves east of U.S. Interstate 35, the damage path noticeably narrows. Large damage gradients are observed along this portion of the damage track. EF4 and EF5 damage is observed just west and east of South Sunnylane Road in eastern Moore. The damage pathlength is 23.25 km. While the path width is quite variable, the maximum width of 1.74 km is located over south Oklahoma City and western Moore.

A more detailed analysis of the initial tornado wind field and attendant damage is shown in Fig. 2. The tornado produced EF4 damage, only 1.42 km from the damage path start, as it passed through a new subdivision, leveling four homes (upper-left inset photo). The damage gradient is quite large. The distance from the centerline to the EF0 isopleth is about 250 m. The photogrammetric funnel-size estimate is much smaller than the damage path width generally coinciding with the EF1 and EF2 isopleths. Previous research has revealed no consistent relationship between the condensation funnel size relative to the damage path width (e.g., Golden and Purcell 1978; Bluestein et al. 1997; Wakimoto et al. 2003). The tornadic wind field based on tree fall and debris is highly convergent toward the centerline. The large convergence is observed at radii (measured from the centerline) close to the funnel edge, suggesting that the tornado radial flow (V_r) is larger than the tangential (V_t). Within the area of the condensation funnel (also lower-right inset photo), cyclonic flow is observed in the tree fall suggesting that $V_t > V_r$.

Radar and visual observations at and just after the time of initial damage (1955:27 UTC) are shown in

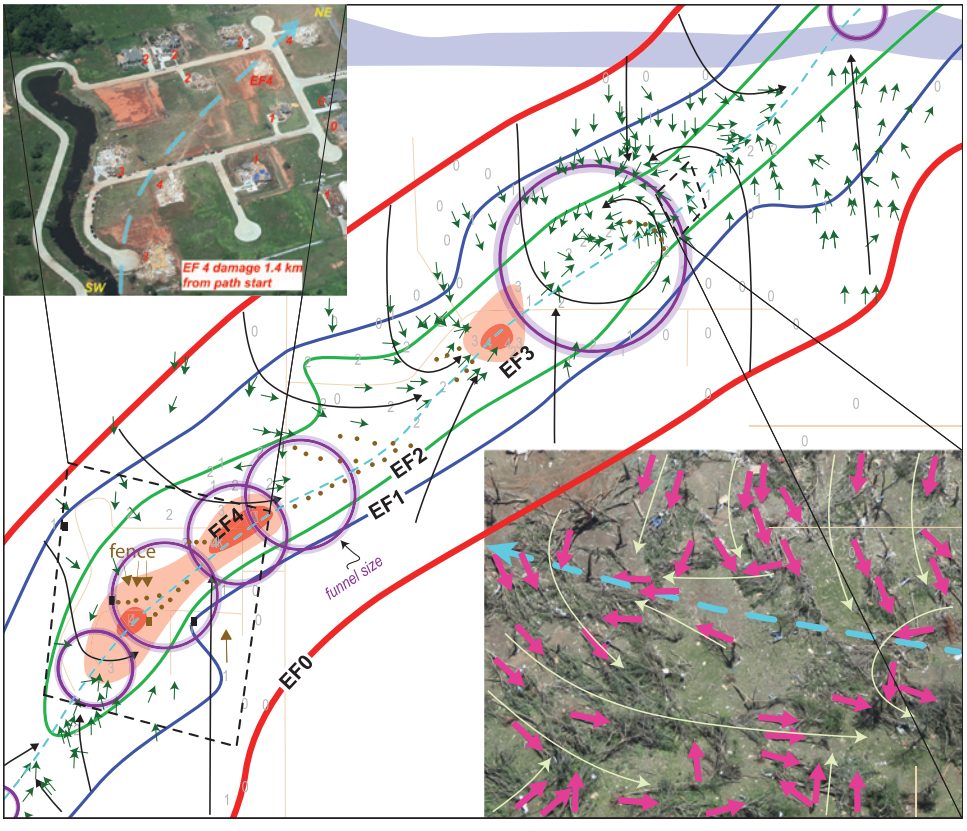

Fig. 2. Damage survey analysis for the dashed magenta box closest to the damage path start in Fig. 1. In addition to the EF-scale isopleths, tree fall (green), EF-scale point values (gray), condensation funnel size (purple) and associated uncertainty (light purple), tornado centerline (cyan), roads (light brown), and debris (brown) are all shown. Brown dots delineate debris paths. Brown arrows represent the direction of debris fall. The black dashed lines delineate the area of the respective aerial photos shown in the inset diagrams. Black curved lines highlight debris and tree fall directions. Point EF-scale values are shown in red in the upper-left inset diagram. In the lower-right inset diagram, tree fall direction (magenta), tornado centerline (cyan), and flow lines (light yellow) are shown.

Figs. 3a–d. The condensation funnel is just making contact with the ground (Fig. 3b). Previous studies have well-documented the ability of dual-polarized radars to detect tornado-generated debris by combining high radar reflectivity (Z_{hh}), very low copolar cross-correlation coefficient (ρ_{hv}), and low differential reflectivity (Z_{DR}) into a tornadic debris signature (TDS; e.g., Ryzhkov et al. 2002, 2005; Bluestein et al. 2007; Kumjian and Ryzhkov 2008; Snyder et al. 2010; Palmer et al. 2011; Bodine et al.

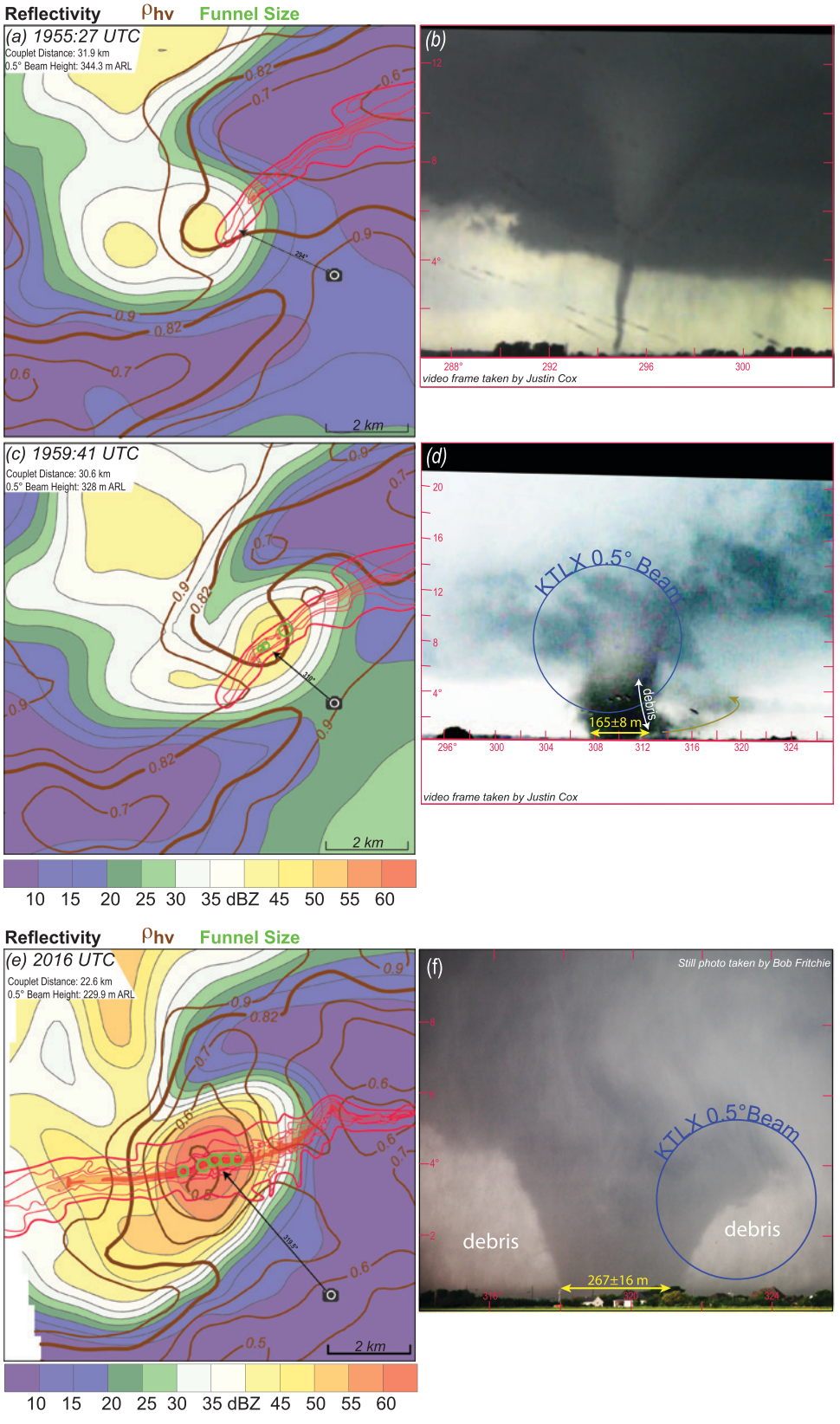

FIG. 3. KTLX radar reflectivity (dBZ; color filled) and copolar cross-correlation coefficient (ρ_{hv}; brown contours) at (a) 1955, (c) 1959, and (e) 2016 UTC. All data are from the 0.5° elevation angle scan. Cross-correlation coefficient is contoured every 0.1. The 0.8 contour has been replaced with 0.82. Also plotted on the radar data are the EF-scale contours from Fig. 1 and condensation funnel sizes (green circles) from photos taken at the approximate time of the radar data. The camera icons indicate the approximate photographer location for photos in (b), (d), and (f). Yellow arrows in the photos are approximate condensation funnel diameters. The brown arrow in (d) is the direction of debris movement. Panels (b) and (d) are video frames taken by Justin Cox. Panel (f) is a still photo taken by Bob Fritchie. The blue circle in (d) and (f) is the approximate dimension and vertical position of the KTLX 0.5° beam.

2013). A Z_{hh} maximum is located near the beginning of the damage track and is collocated with ρ_{hv} values just less than 0.82. Bodine et al. (2013) examined dual-polarization data for two tornadic supercells with accompanying detailed damage surveys and found TDS thresholds for Z_{hh} = 43 dBZ and ρ_{hv} = 0.82 collected at the lowest tilt (0.5°). Using the Bodine et al. (2013) thresholds, the TDS is marginal at the time of tornadogenesis. Four minutes later, the condensation funnel widens (Fig. 3d) and the tornadic winds strengthen, producing EF4 damage to residential structures. Lofted debris, the darkened portion of the condensation funnel in Fig. 3d, is observed near the ground. Video confirms that it is also centrifuged outward, but not carried far above the ground. Despite the observed debris and EF4 damage, the TDS parameters do not change dramatically since 1955 UTC (Fig. 3c). The modest change in the TDS parameters may be explained by the fact that much of the KTLX beam (Fig. 3d) is located above the debris at 1959 UTC.

A portion of the damage path farther east encompassing the Briarwood and Plaza Towers Elementary Schools is shown in Fig. 4. Complete destruction of the Plaza Towers School along with suburban neighborhoods in Moore is evident in the aerial photograph. The small size of the condensation funnel relative to the damage path width is apparent. Highly convergent flow and attendant EF0–3 damage is observed from the outer edge of the damage path to within the condensation funnel. Karstens et al. (2013) also observed strongly convergent flow in tree fall associated with the 2011 Joplin (EF5) and Tuscaloosca–Birmingham (EF4) tornadoes. Lewellen et al. (2000) have simulated low-level tornadic winds that exhibit large ratios of V_r/V_t when the local corner flow swirl ratio is low. Large cyclonic curvature ($V_t > V_r$) is observed within the condensation funnel and generally coincident with the EF3 and EF4 damage near the path centerline (Fig. 4).

Fig. 4. (top) The damage survey analysis as in Fig. 2 for the magenta box in Fig. 1 encompassing South Santa Fe Avenue. (bottom) An aerial photograph looking southwest along the damage path encompassing the Briarwood and Plaza Towers Elementary Schools. EF-scale isopleths have been superimposed for figure clarity.

Radar (2016:43 UTC) and visual observations collected as the tornado approached the Briarwood Elementary School are shown in Figs. 3e and 3f. The Z_{hh} maximum increases in size and intensity since 1959 UTC and is again collocated with the damage track. The ρ_{hv} minimum decreases dramatically to values near 0.5 and is also collocated with the damage track. Striking in Fig. 3e is the relatively small size of the condensation funnel compared to the damage path and TDS. The condensation funnel diameter is estimated to be 18% and 8.4% of the width of the damage path and TDS, respectively. Bluestein et al. (2007) found that the visual extent of a debris cloud generally coincided with ρ_{hv} values indicating debris. Bodine et al. (2013) have shown that the TDS may be much larger than the damage path width. The authors are unaware of any study that has made quantitative comparisons between the dimensions of the collocated condensation funnel, damage path, and TDS.

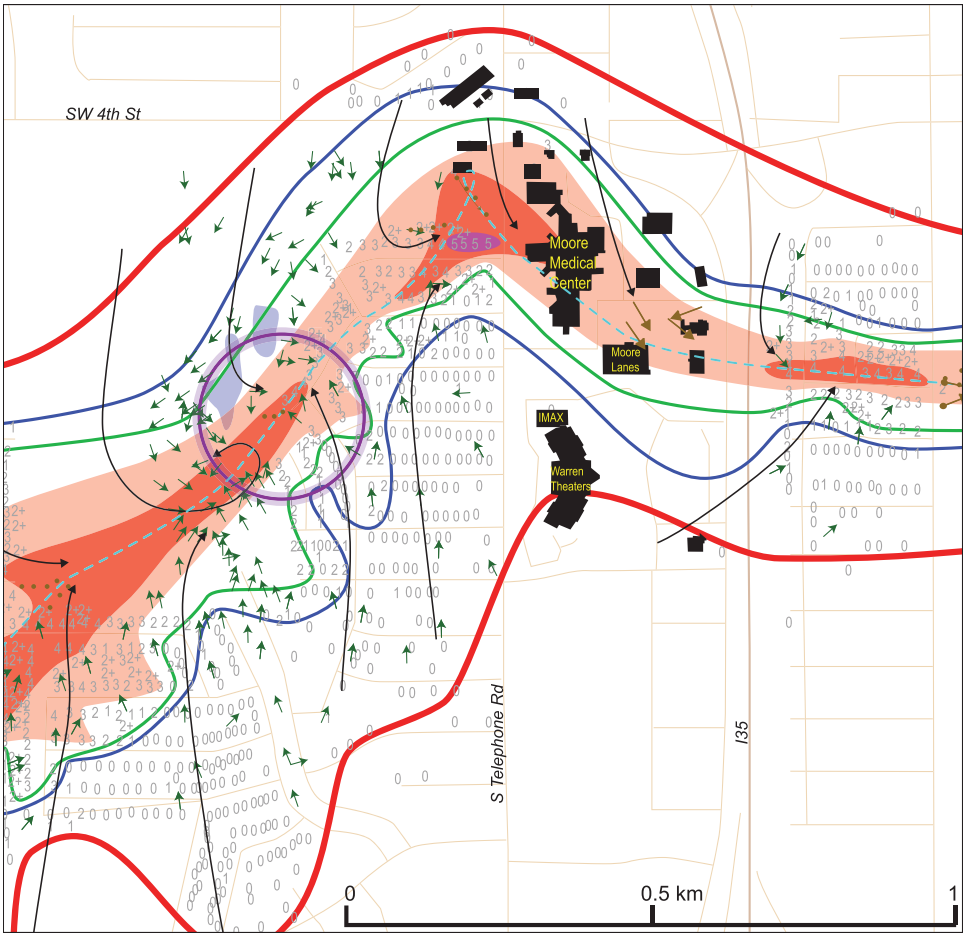

Fig. 5. As in Fig. 2, but for the area in the magenta box in Fig. 1 encompassing U.S. Interstate 35.

A prominent cusp in the damage path with embedded loop of the tornado centerline is observed just west of U.S. Interstate 35 (Fig. 5). The cusps and loops are created as the tornado revolves within its larger-scale parent circulation, the low-level mesocyclone (Fujita 1963; Agee et al. 1976; Brown and Knupp 1980). It is possible that the EF5 damage to the four one- and two-family residential structures just west of the Moore Medical Center is partially a result of the tornado looping just north of their location. These four homes are located on the right side of the tornado (relative to the tornado translation direction) where tornado translation and rotation create the strongest ground-relative wind speeds. The homes also experienced severe, damaging winds for a longer duration in a manner similar to the 1997 Jarrell, Texas, event (Houston and Wilhelmson 2007). The narrowing of the damage path as the tornado moved east of U.S. Interstate 35 is evident in Fig. 5.

The large gradient of damage severity in the damage path between South Eastern and South Bryant Avenues in eastern Moore is evident in Fig. 6. EF4 damage is observed near the tornado centerline (Fig. 6a). Moving either north or south from the centerline, the damage severity decreases by approximately one EF-scale value per house. Strong convergence of the tornadic winds is again implied in the tree fall (Fig. 6a). The only evidence that the Moore tornado may have produced smaller-scale multiple vortices is observed near the Highland East Jr. High School in Figs. 6b and 6c. Swaths of debris north of the tornado centerline and just west of the school are evident. The authors are unaware of any visual or mobile radar data to confirm the presence of multiple vortices associated with the Moore tornado. Video and photos documenting the tornado along the eastern portion of the damage path confirm that it was a single vortex (not shown). It is possible that the debris swaths in Fig. 6 are produced by radial

inflow rolls as discussed in Lewellen and Zimmerman (2008).

Quantifying damage risk. An attempt is made to quantify the risk associated with the Moore tornado and compare it with other well-surveyed EF5 tornadoes. This analysis is motivated by the fact that the tornado damage path data compiled in the storm data, the maximum EF-scale rating, pathlength, and width do not quantify the area experiencing damaging winds for a given EF-scale value. For example, it is not known what fraction of an EF5-rated damage path experiences damage in each of the EF-scale categories. This information will help engineers who are designing tornado-resilient buildings to quantify the number of structures that may survive an EF5 tornado.

Figure 7a illustrates the difference in damage areas between the F5 3 May 1999 Bridge Creek–Moore (Speheger et al. 2002) and the 2013 Moore tornado. The Bridge Creek–Moore tornado encompasses more area for each EF-scale category, attributable to the longer pathlength (61 km). Because the Bridge Creek–Moore tornado traversed more rural area lacking damage indicators compared to the Moore tornado, the respective EF-scale damage areas shown in Fig. 7a may be even larger. Interestingly, the Bridge Creek–Moore tornado damage area increases linearly by about 20% for each successively smaller EF-scale rating, whereas the Moore tornado damage area exponentially increases with decreasing EF-scale rating (Fig. 7b). Abbey and Fujita (1975) observed a similar exponential increase of damage area with decreasing F scale for F5 tornadoes surveyed during the 3 April 1974 Super Outbreak (Fig. 7b). While the generality of these results is not known, they begin to shed some light on the inherent risk associated with EF5 tornadoes. For example, if it is assumed that residential structures rated EF2 or higher are catastrophically damaged, one would expect this over 25% of the total damage area using the 20 May 2013 data.

Comparison between aerial and ground damage surveys. A unique opportunity exists to compare the independent aerial and ground survey results to identify biases. This is especially important in light of recent attempts to use high-resolution aerial and satellite data to map out the damage spatial

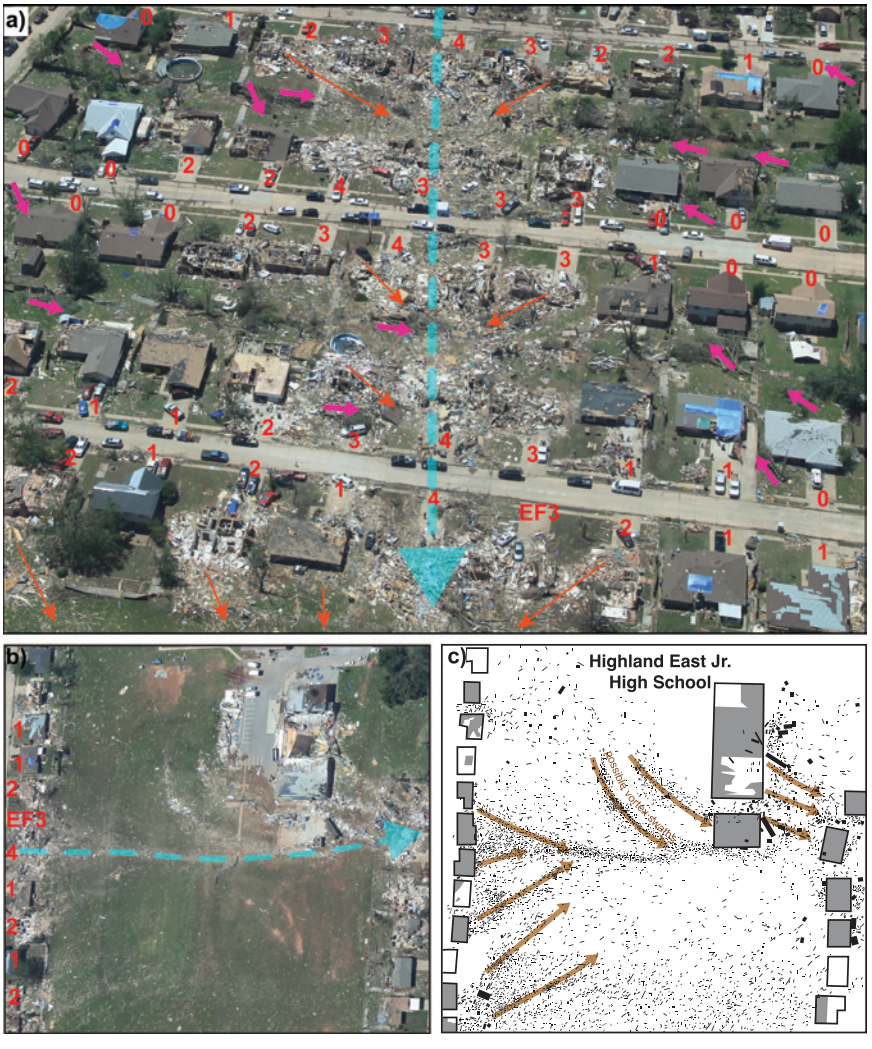

Fig. 6. Aerial photographs in the area of the magenta box in Fig. 1 between South Eastern and Bryant Avenues. (a) Magenta and orange arrows are directions of tree fall and debris, respectively. Large cyan area is the damage path centerline. Red numbers are point EF-scale ratings to structures. (b) Aerial photograph of a field and the Highland East Jr. High School just east of the area shown in (a). Red numbers are the same EF-scale ratings to the easternmost row of homes in (a). (c) Schematic diagram of the debris in (b) and brown arrows showing debris movement by the tornado. The location of possible vortex swaths is also shown. Gray shading in (c) represents damage to structures.

distribution produced by tornadoes (Brown 2010; Edwards et al. 2013). The two surveys analyzed herein are the aerial and ground surveys performed by the authors and the National Weather Center teams, respectively. Both surveys independently identified and rated 4,077 common point structures along the entire damage path. The comparison of over 4,000 common EF ratings in two independent damage surveys is believed to be unprecedented.

Beginning with the ground EF0-rated points (Fig. 8a), while nearly 1,050 points are also rated EF0 in the aerial survey, a large fraction are not identified as damaged (NR = no rating). This is attributed to the ground survey identifying the "threshold of visible damage" or degree of damage 1 (DoD1) to many residential structures that was not visible from the air. A similar low bias in aerial rating is observed for EF1 points. Nearly as many points are rated EF0 as EF1 in the aerial survey. Many of the aerial rated EF0 points are residential structures with minimal roof damage (DoD2). Yet, the ground survey identified "broken glass in windows and doors" (DoD3) or EF1 damage. While it is possible that debris generated by the tornado may be partially responsible for damaging structures in each EF category, it may be especially true for the EF0- and EF1-rated damage that was not obvious in the aerial photographs. The ground and aerial surveys are relatively consistent in rating structures EF2 (Fig. 8c) and EF3 (Fig. 8d) with slightly larger variance in the EF3 ratings. The ground and aerial surveys are very consistent in rating EF4 (Fig. 8e) structures. Quantitative comparison of the small number (11) of structures rated EF5 (Fig. 8f) is not possible. Furthermore, it is not good practice to rate one- and two-family residential structures that appear to be swept clean of the foundation EF5 solely from aerial photographs. A ground assessment of how the structure(s) was built is essential.

SUMMARY AND CONCLUSIONS. An integrated damage, visual, and dual-polarized radar analysis of the 20 May 2013 Moore, Oklahoma, EF5 tornado has been presented. The damage path is 23.25 km long and a maximum width of 1.74 km. Approximately 4,531 structures were damaged by the tornado over an area of 19.04 km^2. The near-surface tornado wind field is characterized by highly convergent flow over the majority of the damage path. At times, it appears that $V_r > V_t$ at radii (measured from the damage path centerline) extending from the EF0 isopleth to less than the outer edge of the condensation funnel.

The KTLX dual-polarized WSR-88D detected a tornado debris signature that is not well correlated with a rapid increase from EF1 to EF4 damage near the time of tornadogenesis. Photogrammetric estimates of debris height from concurrent video observations show that much of the beam was above the debris. While the debris was being centrifuged outward, low-level updrafts were not sufficiently strong enough to loft the debris to heights where it was detectable by KTLX. This is a noteworthy observation as the tornado was only 30 km from the radar. It is possible that the initial debris is not well detected because tornado intensification is much quicker than the time required to loft the debris to

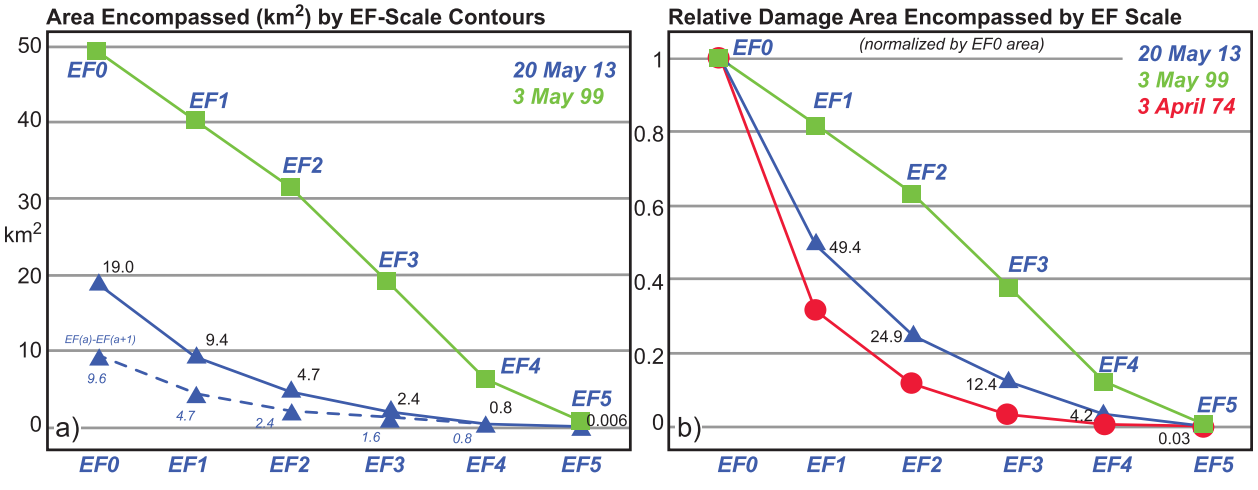

Fig. 7. (a) Area (km^2) encompassed by the respective EF-scale isopleths for the 20 May 2013 Moore and 3 May 1999 Bridge Creek–Moore tornadoes. The blue dashed line is the area of only the respective EF-rated areas (e.g., EF0–EF1). (b) As in (a), but the damage area has been normalized by the respective EF0 areas. Also plotted are data from the 3 Apr 1974 Super Outbreak F5-rated tornadoes. Data for the 3 May 1999 tornado are from Speheger et al. (2002). The 3 Apr 1974 data are from Abbey and Fujita (1975).

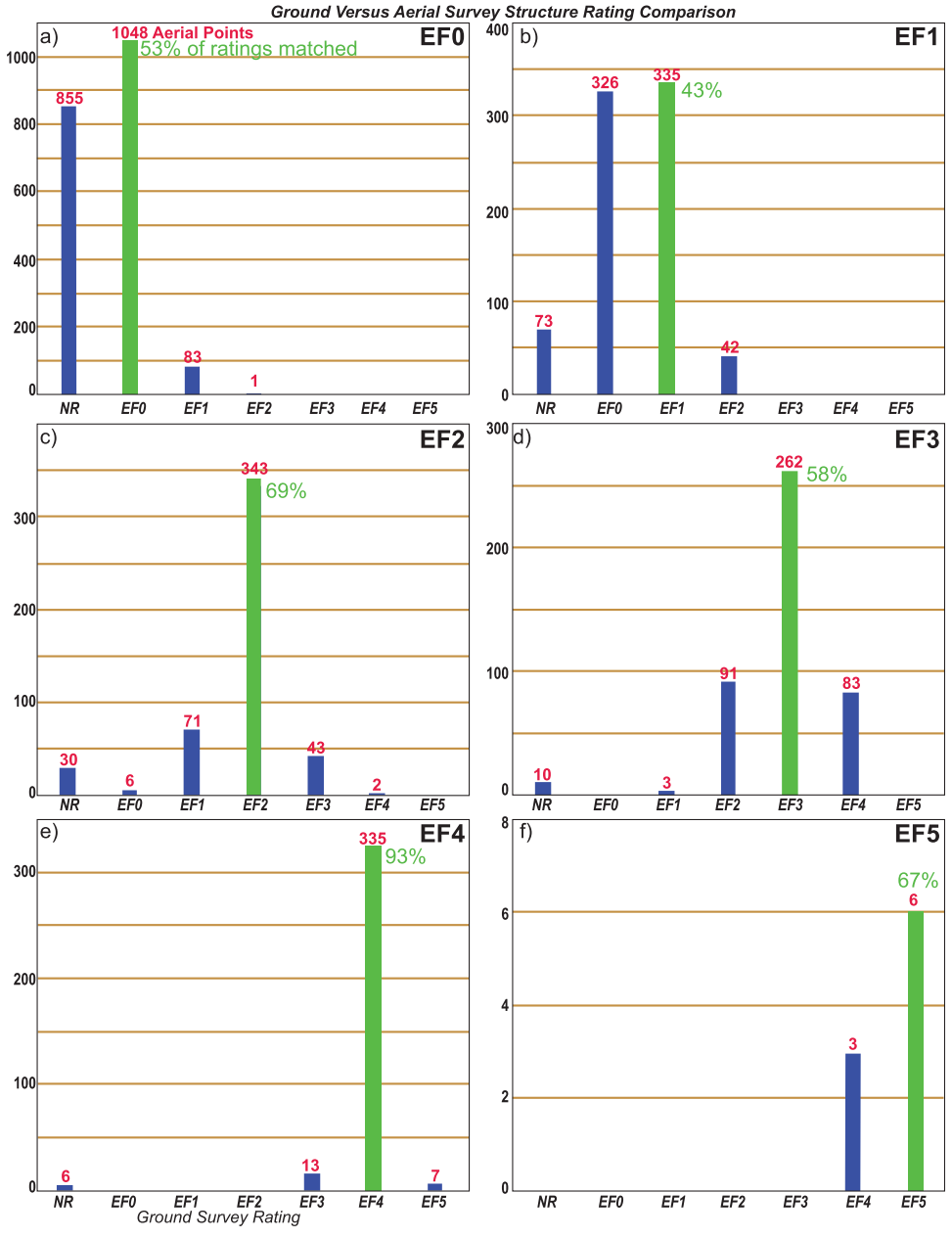

Fig. 8. Comparison of ground and aerial survey ratings for structures in each EF-scale category. In each panel, the abscissa is the ground survey rating. The ordinate is the corresponding number of aerial survey ratings. NR represents structures that were not given a rating in the aerial survey. Percentage in each graph is the number of structures given the same ground and aerial rating. Green bars represent the number of points given the same rating in the ground and aerial surveys.

detectable altitudes. Close to the time of maximum intensity and width, the TDS is well defined and collocated with the damage path and condensation funnel but exhibits a much larger spatial scale due to debris centrifuging. A detailed comparison of the widths of the TDS and condensation funnel and their relationship with the damage path is documented for the first time.

The distribution of damage within the overall path is presented. The damage area increases exponentially with decreasing EF-scale rating. This finding is consistent with F5 tornadoes surveyed as part of the 3 April 1974 Super Outbreak. It differs from the 1999 Bridge Creek–Moore tornado damage area that increases linearly by about 20% for each successively smaller EF-scale rating. Only 25% of the 2013 Moore tornado damage area is rated EF2 or higher.

A comparison of independent ground and aerial damage surveys is presented. The aerial survey contains a low bias for structures rated EF0 and EF1 in the ground survey. This is largely attributed to the difficulty in observing weak damage, DoD1 (EF0) and DoD3 (EF1), to residential structures from overhead aerial photos. It may be possible to see this damage from high-resolution aerial photos taken at low-level oblique angles. Future aerial damage surveys should consider both overhead and oblique viewing angles. Structures rated EF2 and EF3 compare reasonably well given the well-known difficulties of assigning damage ratings to structures (Edwards et al. 2013). Structures rated EF4 are very consistent between the ground and aerial surveys. The small number (10) of structures rated EF5 precludes quantitative comparison.

Despite the apparent low bias in rating residential structures with aerial photographs, future survey

efforts should, if possible, be conducted with both aerial and ground survey teams. In the future, it may be possible to replace aerial survey imagery collected utilizing techniques pioneered by Ted Fujita (e.g., Fujita et al. 1970) with commercially available high-resolution ortho and oblique imagery taken by aircraft and satellites immediately after an event. Ground teams are needed to assess structural engineering integrity, document the role of debris impact, and interview individuals who can offer insight into the structure characteristics and possibly the tornado. On the other hand, aerial surveys can cover the damage path much more quickly. This is especially important for tornado outbreaks or long-track tornadoes where completing detailed ground surveys in a timely manner would not be possible. Covering a damage path quickly and completely is important since debris is often cleaned up immediately after the event. Furthermore, aerial surveys can reveal damage patterns in open terrain such as suction vortex swaths and cusps (e.g., Fujita 1981; Wakimoto et al. 2003) that would not be visible on the ground. This is true for the 31 May 2013 El Reno tornado.

Integrating visual and damage data with close-range dual-polarized radar observations of EF5 tornadoes reveals new insights on the structure and evolution of the tornado, attendant debris, and the low-level wind field. While observations from the KTLX radar are presented herein, other nearby radars, including the Oklahoma City Terminal Doppler Weather Radar (TOKC) collected data during the entire life cycle of the Moore tornado. The range from TOKC to the tornado varied from 5 to 13 km. An important research question concerning tornadoes is observing the near-surface wind field. Future work will focus on retrieving the low-level axisymmetric wind field from the TOKC radar using the ground-based velocity track display (GBVTD) technique (Lee et al. 1999) and compare it with photogrammetric estimates of horizontal and vertical velocities from video and qualitatively with tree fall observations in the damage survey.

ACKNOWLEDGMENTS. A National Science Foundation (NSF) Rapid Response Research (RAPID) Grant (AGS-1343963) supported the results presented herein. Bob Fritchie, Justin Cox, and Chance Coldiron graciously provided photos and video presented herein. Wakimoto was supported by NSF's Independent Research/Development (IRD) activities plan. We thank the National Weather Center Team, and especially Don Burgess, for collaborating on the damage survey.

REFERENCES

Abbey, R. F., Jr., and T. T. Fujita, 1975: Use of tornado path lengths and gradations of damage to assess tornado intensity probabilities. *Preprints, Ninth Conf. on Severe Local Storms*, Norman, OK, Amer. Meteor. Soc., 286–293.

Agee, E. M., J. T. Snow, and P. R. Clare, 1976: Multiple vortex features in the tornado cyclone and the occurrence of tornado families. *Mon. Wea. Rev.,* **104,** 552–563, doi:10.1175/1520-0493(1976)1042.0.CO;2.

Atkins, N. T., A. McGee, R. Ducharme, R. M. Wakimoto, and J. Wurman, 2012: The LaGrange tornado during VORTEX2. Part II: Photogrammetric analysis of the tornado combined with dual-Doppler radar data. *Mon. Wea. Rev.,* **140,** 2939–2958, doi:10.1175/MWR-D-11-00285.1.

Bluestein, H. B., and J. H. Golden, 1993: A review of tornado observations. *The Tornado: Its Structure, Dynamics, Prediction and Hazards, Geophys. Monogr.,* Vol. 79, Amer. Geophys. Union, 319–352.

——, W. P. Unruh, D. C. Dowell, T. A. Hutchinson, T. M. Crawford, A. C. Wood, and H. Stein, 1997: Doppler radar analysis of the Northfield, Texas tornado of 25 May 1994. *Mon. Wea. Rev.,* **125,** 212–230, doi:10.1175/1520-0493(1997)1252.0.CO;2.

——, M. M. French, R. L. Tanamachi, S. Frasier, K. Hardwick, F. Junyent, and A. L. Pazmany, 2007: Close-range observations of tornadoes in supercells made with a dual-polarization, X-band, mobile Doppler radar. *Mon. Wea. Rev.,* **135,** 1522–1543, doi:10.1175/MWR3349.1.

Bodine, D. J., M. R. Kumjian, R. D. Palmer, P. L. Heinselman, and A. V. Ryzhkov, 2013: Tornado damage estimation using polarimetric radar. *Wea. Forecasting,* **28,** 139–158, doi:10.1175/WAF-D-11-00158.1.

Brooks, H. E., and C. A. Doswell III, 2001: Normalized damage from major tornadoes in the United States: 1890–1999. *Wea. Forecasting,* **16,** 168–176, doi:10.1175/1520-0434(2001)0162.0.CO;2.

Brown, T. M., 2010: Development of a statistical relationship between ground-based and remotely-sensed damage in wind storms. Ph.D. dissertation, Texas Tech University, 451 pp.

——, and K. R. Knupp, 1980: The Iowa cyclonic-anticyclonic tornado pair and its parent thunderstorm. *Mon. Wea. Rev.,* **108,** 1626–1646, doi:10.1175/1520-0493(1980)1082.0.CO;2.

Burgess, D. W., and Coauthors, 2014: 20 May 2013 Moore, Oklahoma tornado: Damage survey analysis. *Wea. Forecasting,* in press, doi:10.1175/WAF-D-14-00039.1.

Edwards, R., J. G. LaDue, J. T. Ferree, K. Scharfenberg, C. Maier, and W. L. Coulbourne, 2013: Tornado intensity estimation: Past, present, and future. *Bull. Amer. Meteor. Soc.,* **94,** 641–653, doi:10.1175/BAMS-D-11-00006.1.

Fujita, T. T., 1963: Analytical mesometeorology: A review. *Severe Local Storms, Meteor. Monogr.,* No. 27, Amer. Meteor. Soc., 77–125.

——, 1971: Proposed characterization of tornadoes and hurricanes by area and intensity. University of Chicago SMRP Research Paper 91, 42 pp.

——, 1981: Tornadoes and downbursts in the context of generalized planetary scales. *J. Atmos. Sci.,* **38,** 1511–1534, doi:10.1175/1520-0469(1981)0382.0.CO;2.

——, D. L. Bradbury, and C. F. Van Thullenar, 1970: Palm Sunday tornadoes of April 11, 1965. *Mon. Wea. Rev.,* **98,** 29–69, doi:10.1175/1520-0493(1970)0982.3.CO;2.

Golden, J. H., and D. Purcell, 1978: The life cycle of the Union City, Oklahoma tornado and comparisons with waterspouts. *Mon. Wea. Rev.,* **106,** 3–11, doi:10.1175/1520-0493(1978)1062.0.CO;2.

Houston, A. L., and R. B. Wilhelmson, 2007: Observational analysis of the 27 May 1997 central Texas tornadic event. Part II: Tornadoes. *Mon. Wea. Rev.,* **135,** 727–735, doi:10.1175/MWR3301.1.

Karstens, C. D., W. A. Gallus, B. D. Lee, and C. A. Finley, 2013: Analysis of tornado-induced tree fall using aerial photography from the Joplin, Missouri, and Tuscaloosa–Birmingham, Alabama, tornadoes of 2011. *J. Appl. Meteor. Climatol.,* **52,** 1049–1068, doi:10.1175/JAMC-D-12-0206.1.

Koch, S. E., M. DesJardins, and P. J. Kocin, 1983: An interactive Barnes objective map analysis scheme for use with satellite and conventional data. *J. Climate Appl. Meteor.,* **22,** 1487–1503, doi:10.1175/1520-0450(1983)0222.0.CO;2.

Kumjian, M. R., and A. V. Ryzhkov, 2008: Polarimetric signatures in supercell thunderstorms. *J. Appl. Meteor. Climatol.,* **47,** 1940–1961, doi:10.1175/2007JAMC1874.1.

Kurdzo, J. M., B. L. Cheong, D. J. Bodine, and R. D. Palmer, 2014: The 20 May Newcastle-Moore, Oklahoma EF5 Tornado: High temporal resolution observations using the PX-1000 polarimetric X-band radar. *Special Symp. on Severe Local Storms: The Current State of the Science and Understanding Impacts,* Atlanta, GA, Amer. Meteor. Soc., P824. [Available online at https://ams.confex.com/ams/94Annual/webprogram/Paper231817.html.]

LaDue, J. G., and E. A. Mahoney, 2006: Implementing the new enhanced Fujita scale within the NWS. *23rd Conf. on Severe Local Storms,* St. Louis, MO, Amer. Meteor. Soc., 5.5. [Available online at http://ams.confex.com/ams/pdfpapers/115420.pdf.]

Lee, W.-C., B. J.-D. Jou, P.-L. Chang, and S.-M. Deng, 1999: Tropical cyclone kinematic structure retrieved from single-Doppler radar observations. Part I: Interpretation of Doppler velocity patterns and the GBVTD technique. *Mon. Wea. Rev.,* **127,** 2419–2439, doi:10.1175/1520-0493(1999)1272.0.CO;2.

Lewellen, D. C., and M. I. Zimmerman, 2008: Using simulated tornado surface marks to help decipher near-ground wind fields. *24th Conf. Severe Local Storms,* Savannah, GA, Amer. Meteor. Soc., 8B.1. [Available online at https://ams.confex.com/ams/24SLS/webprogram/Paper141749.html.]

——, W. S. Lewellen, and J. Xia, 2000: The influence of a local swirl ratio on tornado intensification near the surface. *J. Atmos. Sci.,* **57,** 527–544, doi:10.1175/1520-0469(2000)0572.0.CO;2.

Marshall, T. P., 2002: Tornado damage survey at Moore, Oklahoma. *Wea. Forecasting,* **17,** 582–598, doi:10.1175/1520-0434(2002)0172.0.CO;2.

——, K. Jungbluth, and A. Baca, 2008a: The Parkersburg, IA tornado. *24th Conf. Severe Local Storms,* Savannah, GA, Amer. Meteor. Soc., P3.3. [Available online at https://ams.confex.com/ams/24SLS/webprogram/Paper141533.html.]

——, D. McCarthy, J. G. LaDue, J. Wurman, C. R. Alexander, P. Robinson, and K. Kosiba, 2008b: Damage survey and deduction of vortex structure of the Greensburg, KS tornado. *24th Conf. Severe Local Storms,* Savannah, GA, Amer. Meteor. Soc. 8B.3. [Available online at https://ams.confex.com/ams/24SLS/webprogram/Paper141534.html.]

NOAA, 2011: NWS central region service assessment Joplin, Missouri, tornado—May 22, 2011. U.S. Department of Commerce/NOAA/NWS Rep., 41 pp. [Available online at www.nws.noaa.gov/om/assessments/pdfs/Joplin_tornado.pdf.]

Palmer, R. D., and Coauthors, 2011: The 10 May 2010 tornado outbreak in central Oklahoma: Potential for new science with high-resolution polarimetric radar. *Bull. Amer. Meteor. Soc.,* **92,** 871–891, doi:10.1175/2011BAMS3125.1.

Pauley, P. M., and X. Wu, 1990: The theoretical, discrete, and actual response of the Barnes objective analysis scheme for one- and two-dimensional fields. *Mon. Wea. Rev.,* **118,** 1145–1163, doi:10.1175/1520-0493(1990)1182.0.CO;2.

Rasmussen, E. N., R. Davies-Jones, and R. L. Holle, 2003: Terrestrial photogrammetry of weather images acquired in uncontrolled circumstances. *J. Atmos. Oceanic Technol.,* **20,** 1790–1803, doi:10.1175/1520-0426(2003)0202.0.CO;2.

Ryzhkov, A., D. Burgess, D. Zrni, T. Smith, and S. Giangrande, 2002: Polarimetric analysis of a 3 May 1999 tornado. *Preprints, 21st Conf. on Severe Local Storms,* San Antonio, TX, Amer. Meteor. Soc., 14.2. [Available online at https://ams.confex.com/ams/SLS_WAF_NWP/techprogram/paper_47348.htm.]

——, T. J. Schuur, D. W. Burgess, and D. S. Zrnić, 2005: Polarimetric tornado detection. *J. Appl. Meteor.,* **44,** 557–570, doi:10.1175/JAM2235.1.

Simmons, K. M., and D. Sutter, 2011: *Economic and Societal Impacts of Tornadoes.* Amer. Meteor. Soc., 282 pp.

——, and ——, 2012: *Deadly Season: Analysis of the 2011 Tornado Outbreaks.* Amer. Meteor. Soc., 120 pp.

——, ——, and R. Pielke, 2013: Normalized tornado damage in the United States: 1950–2011. *Environ. Hazards,* **12,** 132–147, doi:10.1080/17477891.2012.738642.

Snyder, J. C., H. B. Bluestein, G. Zhang, and S. J. Frasier, 2010: Attenuation correction and hydrometeor classification of high-resolution, X-band, dual-polarized mobile radar measurements in severe convective storms. *J. Atmos. Oceanic Technol.,* **27,** 1979–2001, doi:10.1175/2010JTECHA1356.1.

Speheger, D. A., C. A. Doswell, and G. J. Stumpf, 2002: The tornadoes of 3 May 1999: Event verification in central Oklahoma and related issues. *Wea. Forecasting,* **17,** 362–381, doi:10.1175/1520-0434(2002)0172.0.CO;2.

Wakimoto, R. M., H. V. Murphey, D. C. Dowell, and H. B. Bluestein, 2003: The Kellerville tornado during VORTEX: Damage survey and Doppler radar analyses. *Mon. Wea. Rev.,* **131,** 2197–2221, doi:10.1175/1520-0493(2003)1312.0.CO;2.

——, N. T. Atkins, and J. Wurman, 2011: The LaGrange tornado during VORTEX2. Part I: Photogrammetric analysis of the tornado combined with single-Doppler radar data. *Mon. Wea. Rev.,* **139,** 2233–2258, doi:10.1175/2010MWR3568.1.

WSEC, 2006: A recommendation for an enhanced Fujita scale (EF-scale). Texas Tech University Wind Science and Engineering Center Rep., 111 pp. [Available online at www.depts.ttu.edu/nwi/Pubs/FScale/EFScale.pdf.]

Wurman, J., and C. R. Alexander, 2005: The 30 May 1998 Spencer, South Dakota, storm. Part II: Comparison of observed damage and radar-derived winds in the tornadoes. *Mon. Wea. Rev.,* **133,** 97–119, doi:10.1175/MWR-2856.1.

Zehnder, J. A., J. Hu, and A. Razdan, 2007: A stereo photogrammetric technique applied to orographic convection. *Mon. Wea. Rev.,* **135,** 2265–2277, doi:10.1175/MWR3401.1.

AMS titles now available as eBooks at springer.com

AMS BOOKS

RESEARCH | APPLICATIONS | HISTORY

www.ametsoc.org/amsbookstore

Springer

Scan to see AMS eBook titles at springer.com

AMERICAN METEOROLOGICAL SOCIETY